Nonlinear transformation of waves in finite water depth

James M. Kaihatu[a)]
Fluid Dynamics Branch, Remote Sensing Division (Code 7253), U.S. Naval Research Laboratory, Washington, D.C. 20375

James T. Kirby
Center for Applied Coastal Research, Department of Civil Engineering, University of Delaware, Newark, Delaware 19716

(Received 27 December 1994; accepted 7 April 1995)

The formulation of a nonlinear frequency domain parabolic mild-slope model is detailed. The resulting model describes two-dimensional wave transformation and nonlinear coupling between frequency components. Linear dispersion and transformation characteristics are dictated by fully-dispersive linear theory, an improvement over weakly-dispersive Boussinesq theory. Both the present model and a weakly-dispersive nonlinear frequency domain model are compared to laboratory data for both two-dimensional wave transformation and pure shoaling. It is found that, in general, data-model comparisons are enhanced by the present model, particularly in instances where the wave condition is outside the shallow water range. © *1995 American Institute of Physics.*

I. INTRODUCTION

The Boussinesq equations of Peregrine[1] are often used for nonlinear wave propagation in shallow water. These equations have been treated in both the time domain (e.g. Rygg[2]) and the frequency domain (Freilich and Guza[3]; Liu *et al.*[4]; Kirby[5]). They provide reasonably accurate descriptions of the wavefield provided that the water is sufficiently shallow ($kh \ll 1$, where k is the wavenumber and h the water depth). Unfortunately, errors in wave shoaling and celerity predictions become evident in intermediate or deep water, since the linear dispersion relation and shoaling mechanisms associated with these models become entirely inadequate outside the shallow water range. For example, the "consistent" model of Freilich and Guza[3] (which is a frequency domain treatment of the Boussinesq equations of Peregrine[1] in one dimension) has Green's Law as its shoaling mechanism:

$$\left(\frac{a}{a_0}\right)=\left(\frac{h}{h_0}\right)^{-\frac{1}{4}}. \tag{1}$$

This dictates a monotonic increase in wave amplitude a with a decrease in h. Applying this shoaling relation to a typical wind-wave spectrum would result in overshoaling in frequency components which are in either intermediate or deep water, where kh is not small.

In this study we wish to derive a nonlinear frequency domain parabolic mild-slope equation. This model would have the correct linear dispersion and shoaling characteristics (i.e., that of fully-dispersive linear theory), while retaining nonlinear coupling between frequency components. Several investigators have previously worked on models similar to the one described herein. Bryant[6,7] formulated a model from the boundary value problem for water waves over a flat bottom by specifying spatially periodic Fourier expansions for the variables ϕ and η which satisfy the Laplace equation and the bottom boundary condition, substituting these into the two free surface boundary conditions, and then integrating to solve for the amplitude coefficients, which vary slowly in time. The interaction coefficients which determine the degree of energy exchange among resonant triads were derived without restrictions on the size of the dispersion parameter kh. However, the time varying, spatially periodic formulation is not suitable for most applications, since wave information is usually taken in the form of time series from stationary gauges. These data are processed and stored by means of a frequency-domain Fast Fourier Transform (FFT), which presupposes equal intervals of frequencies rather than wave numbers. Additionally, the waves over varying bathymetry can evolve rapidly in space, precluding the assumption of spatial periodicity. Keller[8] developed a set of equations describing the evolution of two interacting wave components. He demonstrated that, in the nondispersive limit, this same set of evolution equations can be derived from the exact Euler equations, the nonlinear shallow water equations, and the Boussinesq equations. The model described in this paper would match his model before the nondispersive limit is taken if the number of frequency components is truncated to two and slow time dependence is reincorporated. Keller[8] did not model his equations. Agnon *et al.*[9] derived a one-dimensional nonlinear shoaling model for time periodic, spatially varying waves from the boundary value problem.

We take a different approach in the present study to derive what is essentially a two-dimensional extension of the model of Agnon *et al.*[9] We begin with the boundary value problem for water waves and derive the basic model in Section II. In Section III we assume periodicity in time and transform the problem into the frequency domain by factoring out the time dependence, resulting in a nonlinear elliptic mild-slope equation. In the process we explicitly formulate the nonlinear coupling between frequency modes. Section IV details the use of the parabolic approximation to develop two-dimensional evolution equations governing the spectral amplitudes. We show comparisons of the resulting model to both experimental data and weakly-dispersive spectral trans-

a)E-mail: kaihatu@shredder.nrl.navy.mil

 1070-6631/95/7(8)/1903/12/$6.00

formation models in Section V. We present conclusions and propose extensions of the work in Section VI. In Appendix A 1 we present an alternative derivation of the basic model using the Lagrangian for water waves. In keeping with the general nature of the discussion, we extend this formulation to include the effects of ambient currents in Appendix A 2.

II. BOUNDARY VALUE PROBLEM

We consider a wavefield propagating over a spatially varying bottom. The Cartesian coordinate system (x,y,z) is located on the still-water level, with z considered positive upwards from the origin. The wavefield is denoted in terms of the free surface elevation $\eta(x,y,t)$ (where t is time) which is defined from the still water level $z=0$. The water depth is denoted $h(x,y)$. The fluid is assumed to be inviscid and irrotational. In concert with this assumption, we use the water wave boundary value problem for the velocity potential ϕ:

$$\nabla^2\phi=\nabla_h^2\phi+\phi_{zz}=0; \quad -h\leqslant z\leqslant\eta, \tag{2}$$

$$\phi_z=-\nabla_h h\cdot\nabla_h\phi; \quad z=-h, \tag{3}$$

$$g\eta+\phi_t+\tfrac{1}{2}(\nabla_h\phi)^2+\tfrac{1}{2}(\phi_z)^2=0; \quad z=\eta, \tag{4}$$

$$\eta_t-\phi_z+\nabla_h\eta\cdot\nabla_h\phi=0; \quad z=\eta, \tag{5}$$

where ∇_h denotes the gradient operation in the horizontal coordinates (x,y) and g is the gravitational acceleration. Subscripts denote differentiation.

We wish to retain leading order nonlinearity in the free surface boundary conditions. Rather than scale and nondimensionalize the problem, we instead follow the approach of Bryant[6] and retain dimensional quantities, with the understanding that leading order nonlinearity is $O(\epsilon^2)$, where $\epsilon(=ka$, where a is a characteristic wave amplitude) is the nonlinearity parameter. We note here that the scaled, nondimensionalized problem had been addressed by Agnon *et al.*;[9] the approach here is entirely equivalent.

The free surface boundary conditions are both nonlinear and applied at a position not known *a priori*; thus we expand these in Taylor series about $z=0$ and retain terms to $O(\epsilon^2)$. The truncated boundary value problem is now:

$$\nabla_h^2\phi+\phi_{zz}=0; \quad -h\leqslant z\leqslant 0, \tag{6}$$

$$\phi_z=-\nabla_h h\cdot\nabla_h\phi; \quad z=-h, \tag{7}$$

$$g\eta+\phi_t+\tfrac{1}{2}(\nabla_h\phi)^2+\tfrac{1}{2}(\phi_z)^2+\eta\phi_{zt}=O(\epsilon^3); \quad z=0, \tag{8}$$

$$\eta_t-\phi_z+\nabla_h\eta\cdot\nabla_h\phi-\eta\phi_{zz}=O(\epsilon^3); \quad z=0. \tag{9}$$

Instead of using the approach of Bryant,[6] who substituted an appropriate form for ϕ that would satisfy the Laplace equation and the bottom boundary condition, we instead use the approach of Smith and Sprinks,[10] who used Green's second identity to derive a linear mild-slope equation. We first assume a superposition of solutions:

$$\phi(x,y,z,t)=\sum_{n=1}^{N} f_n(k_n,h,z)\tilde{\phi}_n(k_n,\omega_n,x,y,t), \tag{10}$$

where ω_n is the radian frequency and k_n is the wave number of the nth frequency component, and:

$$f_n=\frac{\cosh k_n(h+z)}{\cosh k_n h} \tag{11}$$

or the usual depth dependence dictated by linear theory. The frequency ω_n and the wave number k_n are related by the linear dispersion relation:

$$\omega_n^2=gk_n\tanh k_n h. \tag{12}$$

It is convenient to combine the two surface boundary conditions (8) and (9) into a single equation for ϕ only. Eliminating η from the surface boundary conditions leads to:

$$\phi_z=-\frac{1}{g}\Big[\phi_{tt}+\frac{1}{2}(\nabla_h\phi)_t^2+\tfrac{1}{2}(\phi_z)_t^2-\frac{1}{2g}(\phi_t)_{zt}^2 +\nabla_h\cdot(\phi_t\nabla_h\phi)\Big]; \quad z=0. \tag{13}$$

In the manner of Smith and Sprinks,[10] we will use Green's second identity on the variables f_n and $\tilde{\phi}_n$, as follows:

$$\nabla_h\cdot\left(\int_{-h}^{0} f_n^2 dz\nabla_h\tilde{\phi}_n\right)-\int_{-h}^{0} f_{nz}^2 dz\tilde{\phi}_n =-f_n\tilde{\phi}_{nz}|_{z=0}+O(\epsilon,\tilde{\alpha}^2) \tag{14}$$

where $\tilde{\alpha}$ is a parameter characterizing the bottom slope. For our purposes it is assumed that

$$\tilde{\alpha}\leqslant O(\epsilon). \tag{15}$$

In this manner we can eliminate bottom boundary terms in comparison to $O(\epsilon^2)$ terms from the free surface. Development of the linear part of the models is identical to Smith and Sprinks;[10] reference is made to their paper. We simply note that:

$$f_n(0)=1, \tag{16}$$

$$f_{nz}(0)=\frac{\omega_n^2}{g}, \tag{17}$$

$$\int_{-h}^{0} f_n^2 dz=\frac{(CC_g)_n}{g}, \tag{18}$$

$$\int_{-h}^{0}(f_{nz})^2 dz=\frac{\omega_n^2}{g}\left(1-\frac{C_{gn}}{C_n}\right), \tag{19}$$

where C_n is the wave celerity and C_{gn} the group velocity of the nth component. The subscript z refers to partial differentiation with respect to z. Substitution of (10), (13), (16), (17), (18), and (19) into (14) and manipulation of the integrals yields a time-dependent mild-slope equation with nonlinear coupling between modes:

$$\tilde{\phi}_{n_{tt}} - \nabla_h \cdot [(CC_g)_n \nabla_h \tilde{\phi}_n] + \omega_n^2 \left(1 - \frac{C_{gn}}{C_n}\right) \tilde{\phi}_n$$
$$= \frac{1}{2} \Bigg\{ \sum_l \sum_m \left[\frac{\omega_l^2 + \omega_m^2}{g^2} (\tilde{\phi}_{l_t} \tilde{\phi}_{m_t})_t - \frac{\omega_l^2 \omega_m^2}{g^2} (\tilde{\phi}_l \tilde{\phi}_m)_t \right]$$
$$- \sum_l \sum_m [(\nabla_h \tilde{\phi}_l \cdot \nabla_h \tilde{\phi}_m)_t + \nabla_h \cdot (\tilde{\phi}_{l_t} \nabla_h \tilde{\phi}_m)$$
$$+ \nabla_h \cdot (\tilde{\phi}_{m_t} \nabla_h \tilde{\phi}_l)] \Bigg\}_n , \tag{20}$$

where the notation $\{\}_n$ on the right-hand side of (20) indicates that the nonlinear coupling occurs between the mode under consideration (n) and two other modes in the spectrum (l and m). Explicit relationships between l, m, and n follow the rules of resonant triad interaction theory (Phillips[11]). These restrictions will be imposed in the next section.

Despite the fact that we have decomposed the wavefield into individual components, we have not made any assumptions concerning the behavior of these components; they could represent propagating or standing waves with characteristics that vary slowly in time and space. It is noted here that, in the linear limit, (20) approaches a representation of decoupled, independent waves. In the shallow water limit (as $k_n h$ approaches zero) we approach a frequency domain representation of Boussinesq-type shallow water waves, as discussed by Freilich and Guza.[3] Additionally, Bryant[7] showed that a system like (20), with coefficients expressed as a power series in ϵ, will join smoothly to a solution for Stokes waves in deep water for $N=3$ components.

III. TIME-HARMONIC WAVE PROPAGATION IN TWO DIMENSIONS

We wish to develop a series of evolution equations for the propagation of time-harmonic waves in two spatial dimensions. Hence, we can completely factor out the time dependence by assuming:

$$\tilde{\phi}_n(x,y,t) = \frac{\hat{\phi}_n}{2} e^{-i\omega_n t} + \frac{\hat{\phi}_n^*}{2} e^{i\omega_n t} \tag{21}$$

and using resonant triad interactions to formulate the nonlinear coupling between frequency components (e.g. Phillips[11]). This yields a time-harmonic wave equation with modification by nonlinearity:

$$\nabla_h \cdot [(CC_g)_n \nabla_h \hat{\phi}_n] + k_n^2 (CC_g)_n \hat{\phi}_n = -\frac{i}{4} \Bigg[\sum_{l=1}^{n-1} 2\omega_n \nabla_h \hat{\phi}_l \cdot \nabla_h \hat{\phi}_{n-l} + \omega_l \hat{\phi}_l \nabla_h^2 \hat{\phi}_{n-l} + \omega_{n-l} \hat{\phi}_{n-l} \cdot \nabla_h^2 \hat{\phi}_l + \frac{\omega_l \omega_{n-l} \omega_n}{g^2}$$
$$\times (\omega_l^2 + \omega_l \omega_{n-l} + \omega_{n-l}^2) \hat{\phi}_l \hat{\phi}_{n-l} \Bigg] - \frac{i}{2} \Bigg[\sum_{l=1}^{N-n} 2\omega_n \nabla_h \hat{\phi}_l^* \cdot \nabla_h \hat{\phi}_{n+l} + \omega_{n+l} \hat{\phi}_{n+l} \nabla_h^2 \hat{\phi}_l^*$$
$$- \omega_l \hat{\phi}_l^* \nabla_h^2 \hat{\phi}_{n+l} - \frac{\omega_l \omega_{n+l} \omega_n}{g^2} (\omega_l^2 - \omega_l \omega_{n+l} + \omega_{n+l}^2) \hat{\phi}_l^* \hat{\phi}_{n+l} \Bigg] . \tag{22}$$

We note here that the solution of Bryant[6] can be recovered by assuming spatial (rather than temporal) periodicity in (20). While we have incorporated an assumption of time periodicity into our problem, we have still not explicitly specified the spatial variation of the wavefield. Additionally, (22) is elliptic, with the linear terms comprising the elliptic mild-slope equation model of Berkhoff[12] and Smith and Sprinks.[10] Numerical solution of the equation in this form would require fine resolution (many gridpoints per wavelength) and complete specification of the boundary. This is not well suited for coastal propagation problems in which the shoreline location is not known *a priori* and the modeled region can be on the order of kilometers in size.

IV. PARABOLIC APPROXIMATION

We will restrict the problem to that of a progressive wave field with the following form:

$$\hat{\phi}_n(x,y) = -\frac{ig}{\omega_n} A_n(x,y) e^{i\int k_n(x,y)dx}, \tag{23}$$

$$\hat{\phi}_n^*(x,y) = \frac{ig}{\omega_n} A_n^*(x,y) e^{-i\int k_n(x,y)dx}, \tag{24}$$

where the complex amplitude A_n is assumed to be a slowly varying function of the spatial coordinates (x,y), and the wave is assumed to be traveling primarily in the $+x$ direction. Substituting (23) and (24) into (22) gives:

$$[(CC_g)_n A_{nx}]_x + 2i(kCC_g)_n A_{nx} + i(kCC_g)_{nx} A_n$$
$$+ [(CC_g)_n (A_n e^{i\int k_n(x,y)dx})_y]_y e^{-i\int k_n(x,y)dx}$$
$$= \frac{1}{4} \sum_{l=1}^{n-1} R A_l A_{n-l} e^{i\int (k_l + k_{n-l} - k_n)dx}$$
$$+ \frac{1}{2} \sum_{l=1}^{N-n} S A_l^* A_{n+l} e^{i\int (k_{n+l} - k_l - k_n)dx}, \tag{25}$$

where

$$R(\omega_n,\omega_{n-l},\omega_l,k_{n-l},k_l)$$

$$=\frac{g}{\omega_l\omega_{n-l}}[\omega_n^2k_lk_{n-l}+(k_l+k_{n-l})(\omega_{n-l}k_l+\omega_lk_{n-l})\omega_n]$$

$$-\frac{\omega_n^2}{g}(\omega_l^2+\omega_l\omega_{n-l}+\omega_{n-l}^2), \tag{26}$$

$$S(\omega_n,\omega_{n+l},\omega_l,k_{n+l},k_l)$$

$$=\frac{g}{\omega_l\omega_{n+l}}[\omega_n^2k_lk_{n+l}+(k_{n+l}-k_l)(\omega_{n+l}k_l+\omega_lk_{n+l})\omega_n]$$

$$-\frac{\omega_n^2}{g}(\omega_l^2-\omega_l\omega_{n+l}+\omega_{n+l}^2). \tag{27}$$

Because (25) is still elliptic, we need to explicitly invoke the parabolic approximation (Radder;[13] Lozano and Liu[14]). We have assumed that the wave propagates primarily in the $+x$-direction; thus we retain fast wave-like variations in the x-direction but not in the y-direction. The fast variations in the x-direction are accounted for by the complex exponential in (23) and (24). We use the scaling approach of Yue and Mei[15] to order the derivatives of A_n as follows:

$$\frac{\partial A_n}{\partial x}=O(\epsilon^2), \tag{28}$$

$$\frac{\partial A_n}{\partial y}=O(\epsilon), \tag{29}$$

since the fast variations in x have already been factored out. The ordering of the y-derivative in (29) allows us to keep $\partial^2A_n/\partial y^2$, thereby allowing us to model the slow phase-like variations of the wave in the y-direction that occur when it is turned at a small angle to the x-direction. Additionally, since we assume the wave to propagate primarily in the x-direction, changes in the amplitude A_n would be due mostly to x-derivatives of the depth h. Thus, the order of bottom slope in the x-direction (h_x), as well as x-derivatives of depth-dependent properties (e.g., C, C_g), should also be $O(\epsilon^2)$. This allows us to order the relative amplitudes of the first two terms of (25) as:

$$\epsilon^4[(CC_g)_nA_{nx}]_x\ll\epsilon^2[2i(kCC_g)_nA_{nx}], \tag{30}$$

where the subscript x refers to differentiation with respect to x. Since we are keeping terms to $O(\epsilon^2)$ we drop the first term in (25). Additionally, we need to factor out any y dependence from the phase function. This must be done since we are only integrating the phase in x, but the wave number k_n is a function of both x and y. There are several ways to address this; we choose the method of Lozano and Liu,[13] where they defined a y-averaged wave number $\bar{k}_n(x)$ as a reference phase function. Thus, we rewrite (23) and (24) as:

$$\hat{\phi}_n(x,y)=-\frac{ig}{\omega_n}a_n(x,y)e^{i\int\bar{k}_n(x)dx}, \tag{31}$$

$$\hat{\phi}_n(x,y)=\frac{ig}{\omega_n}a_n^*(x,y)e^{-i\int\bar{k}_n(x)dx}, \tag{32}$$

which gives:

$$A_n(x,y)=a_n(x,y)e^{i(\int\bar{k}(x)_ndx-\int k_n(x,y)dx)} \tag{33}$$

and:

$$A_n^*(x,y)=a_n^*(x,y)e^{-i(\int\bar{k}(x)_ndx-\int k_n(x,y)dx)}. \tag{34}$$

Substituting this into (25) yields:

$$2i(kCC_g)_na_{nx}-2(kCC_g)_n(\bar{k}_n-k_n)a_n+i(kCC_g)_{nx}a_n$$

$$+[(CC_g)_n(a_n)_y]_y$$

$$=\frac{1}{4}\left(\sum_{l=1}^{n-1}Ra_la_{n-l}e^{i\int(\bar{k}_l+\bar{k}_{n-l}-\bar{k}_n)dx}\right.$$

$$\left.+2\sum_{l=1}^{N-n}Sa_l^*a_{n+l}e^{i\int(\bar{k}_{n+l}-\bar{k}_l-\bar{k}_n)dx}\right). \tag{35}$$

The two-dimensional parabolic equation (35) was modeled with the Crank–Nicholson numerical scheme. This scheme is unconditionally stable for linear problems, and is second-order accurate in x and y. The parabolic model (35) was converted to finite differences much like the Kadomtsev–Petviashvili (KP) model of Liu *et al.*,[4] where the numerical scheme was detailed; thus, it will not be shown here. For the case of unidirectional wave shoaling we reduce the model to one dimension:

$$A_{nx}+\frac{(kCC_g)_{nx}}{2(kCC_g)_n}A_n$$

$$=-\frac{i}{8(kCC_g)_n}\left(\sum_{l=1}^{n-1}RA_lA_{n-l}e^{i\int(k_l+k_{n-l}-k_n)dx}\right.$$

$$\left.+2\sum_{l=1}^{N-n}SA_l^*A_{n+l}e^{i\int(k_{n+l}-k_l-k_n)dx}\right) \tag{36}$$

where we revert back to the A_n notation since the reference wave number $\bar{k}_n$ is identical to k_n. This one-dimensional model is identical to that of Agnon *et al.*,[9] which was derived using continuous Fourier integrals rather than discrete Fourier transforms, as we have done here. We model (36) with a fourth-order Runge–Kutta scheme with error checking and adjustable stepsize control.

V. COMPARISONS TO DATA

To verify the performance of the model, we will compare it to available experimental data. The first comparison will be to the data of Whalin,[16] who conducted a laboratory experiment to investigate the limits of linear refraction theory. He generated sinusoidal waves of 1, 2, and 3 second periods and ran them over bathymetry that resembled a tilted cylinder. The bottom contours and tank dimensions are shown in Figure 1. We only compare the 2 and 3 second cases; the 1 second case will be discussed later in this section. The wave parameters for the cases used in the comparison are shown in Table I, where the tank depth used in cal-

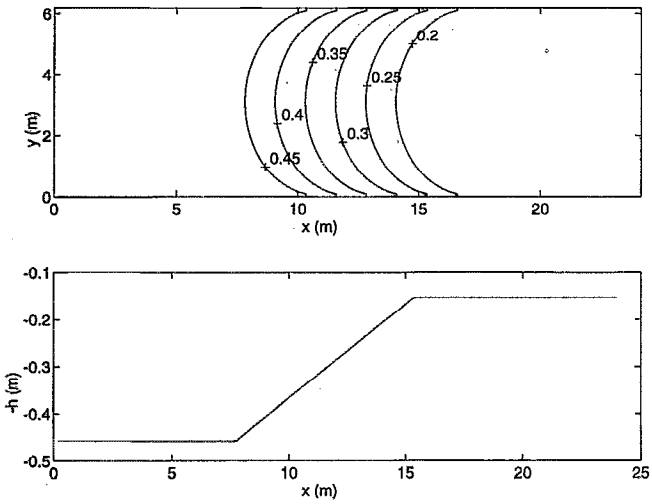

FIG. 1. Wavetank layout of experiment of Whalin.[16] (Top) bottom contours; (bottom) centerline depth.

culating the nonlinearity parameter ka and the dispersion parameter kh were chosen to maximize the values of these parameters [k was calculated by (12) using the primary harmonic]. Whalin[16] placed gages at certain locations along the centerline, and recorded the amplitudes of the first three harmonics. This experiment demonstrated the inadequacy of non-diffractive linear refraction theory as a general modeling methodology; wave ray crossing downwave of the top of the tilted cylinder would indicate an infinite waveheight according to linear refraction theory, which would be impossible. Diffraction is very prevalent there. Additionally, using a linear sinusoidal wave as input generates higher harmonics since the nonlinear surface boundary conditions cannot be satisfied by a single harmonic.

We ran the parabolic nonlinear mild-slope model (35) and the KP parabolic frequency domain model of Liu *et al.*[4] against the data of Whalin using the parameters shown in Table I. This KP model is essentially a frequency domain treatment of a reduction of the Boussinesq equations of Peregrine,[1] and so has lowest-order dispersion and Green's Law shoaling. We used $N=5$ harmonics for the $T=3$ second case and $N=3$ harmonics for $T=2$ seconds. A grid spacing of $\Delta x=12$ cm and $\Delta y=8$ cm was used for both models. No substantial improvements were noted when the stepsizes were halved.

TABLE I. Wave parameters of experiment of Whalin[16] used in data-model comparisons ($h_1=45.7$ cm; $h_2=15.2$ cm).

T (sec)	a_0 (cm)	ka	kh_1
3	0.68	0.0068	0.464
3	0.98	0.0098	0.464
3	1.46	0.0146	0.464
2	0.75	0.0120	0.733
2	1.06	0.0169	0.733
2	1.49	0.0238	0.733

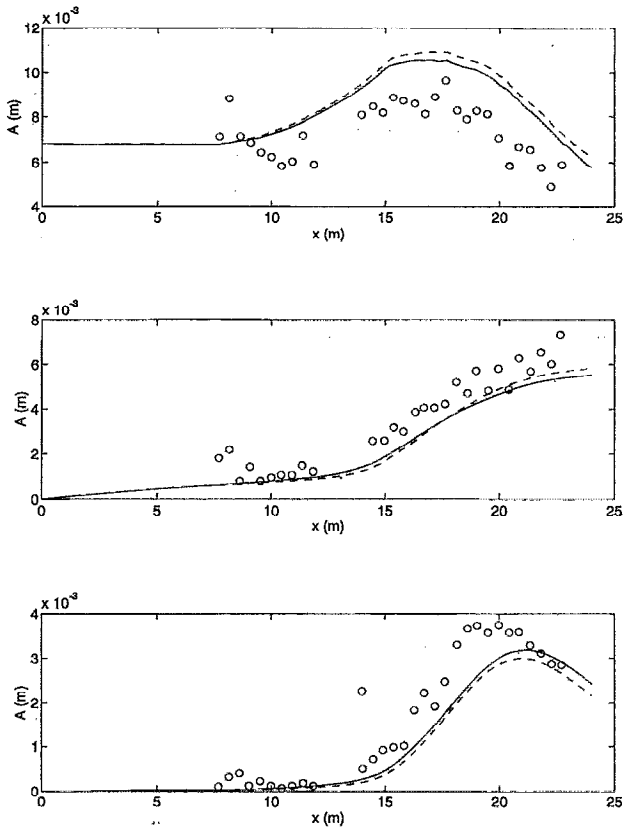

FIG. 2. Comparisons between models and Whalin's experiment, $T=3$ s, $a_0=0.68$ cm. Nonlinear mild-slope model (–), KP model of Liu *et al.*[4] (– –), data of Whalin[16] (○). (Top) first harmonic; (middle) second harmonic; (bottom) third harmonic.

Figures 2 through 4 show the comparisons between the models and Whalin's data for the case of $T=3$ seconds. It is apparent that neither model predicts the first harmonic amplitudes particularly well. This seems to be endemic of most data-model comparisons done in the literature where Whalin's $T=3$ second data were used (e.g., Rygg;[2] Madsen and Sørensen;[17] Nwogu[18]). Liu *et al.*[4] maintain that the relatively short evolution distance for a 3 second wave period (roughly two wavelengths) may at least partially violate the slowly varying assumption used to derive their frequency domain KP model. In any case, both models show reasonable comparison with the $T=3$ second data for the second and third harmonics.

The $T=2$ second case is more demonstrative of the advantages of the dispersive model. The value of the dispersion parameter kh in the deep portion of the tank is 0.733, which may violate the shallow water assumption used in the KP model of Liu *et al.*[4] Figures 5 through 7 show these results. It is apparent that (35) models the first harmonic amplitudes better than the KP model. The overprediction of these amplitudes by the KP model is most likely due to the inherent Green's Law shoaling. The prediction of the second and third harmonic amplitudes are equivalent between the two models, despite the relatively high values of kh in the deep portion of

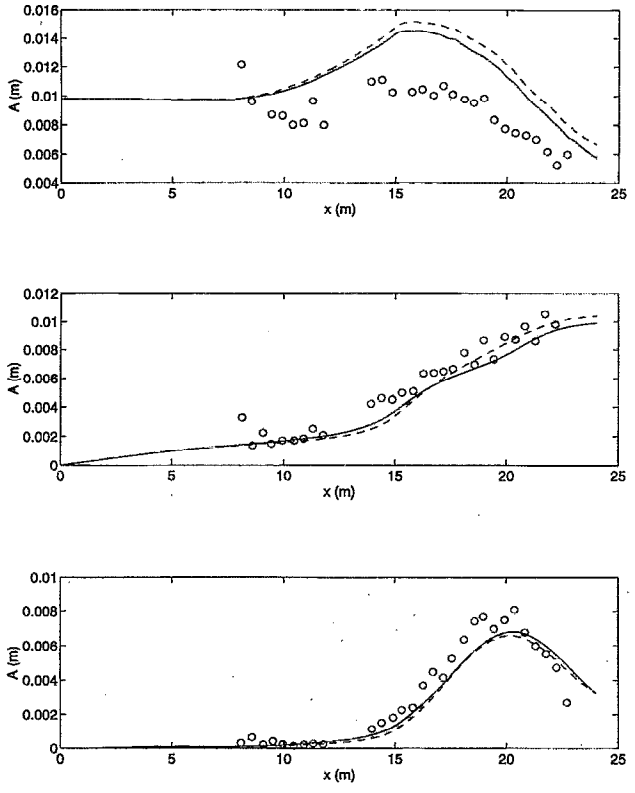

FIG. 3. Comparisons between models and Whalin's experiment, $T=3$ s, $a_0=0.98$ cm. Nonlinear mild-slope model (–), KP model of Liu *et al.*[4] (– –), data of Whalin[14] (O). (Top) first harmonic; (middle) second harmonic; (bottom) third harmonic.

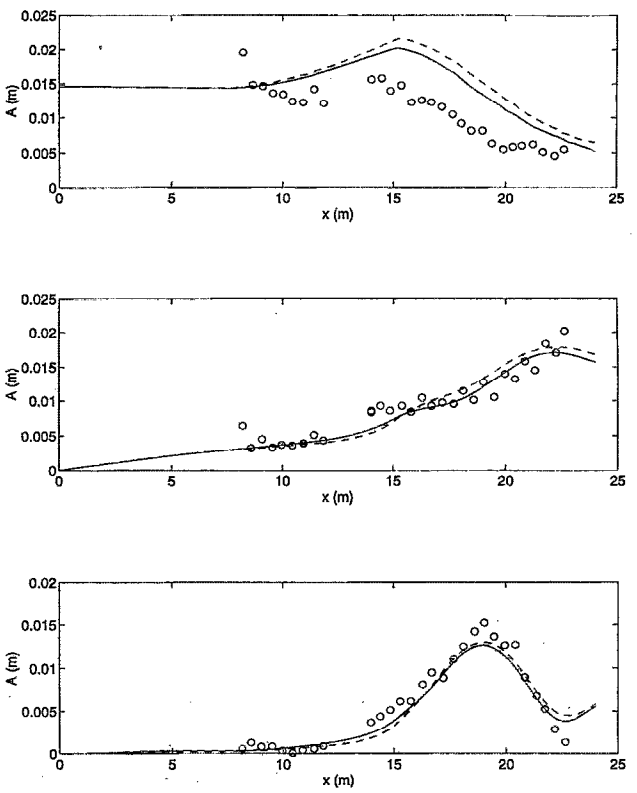

FIG. 4. Comparison between models and Whalin's experiment, $T=3$ s, $a_0=1.46$ cm. Nonlinear mild-slope model (–), KP model of Liu *et al.*[4] (– –), data of Whalin[16] (O). (Top) First harmonic; (middle) Second harmonic; (bottom) third harmonic.

the tank ($kh=1.92$ for the second harmonic and $kh=4.94$ for the third). This equivalence may be due to the fact that these harmonics are input with zero amplitude and allowed to grow initially due to nonlinear energy exchange between components. For such a relatively short slope, it is possible that nonlinearity, rather than first-order quantities like shoaling and refraction, control the evolution of these harmonic amplitudes, and as such are not affected by the disparity between a dispersive shoaling mechanism and Green's Law. This would not be the case for a broad spectrum of irregular waves shoaling over a long slope, as we shall see in the next set of comparisons.

It can be argued that the $T=1$ second case of Whalin[16] would be a more severe test case for (35). The value of kh for this case is 1.92 in the deep portion of the tank. Both Madsen and Sørensen[17] and Nwogu[18] compared their time domain dispersive Boussinesq equations to this case; they both demonstrate reasonable agreement with the data. However, the effectiveness of the frequency domain formulation used here is contingent upon the relative size of the arguments of the complex exponentials in the nonlinear right-hand side of (35). These arguments can become large in deep water, invalidating the assumption of slow spatial variation used in deriving the model. This problem will likely arise in the simulation of the $T=1$ second case; thus we do not compare our model to it. We feel, however, that the favorable results demonstrated by the $T=2$ second case is sufficient attestation to the importance of incorporating dispersion and shoaling characteristics in nonlinear wave transformation which are valid for arbitrary water depth.

We also compare our one-dimensional model (36) to Case 2 of the wave shoaling experiment of Mase and Kirby.[19] This experiment was conducted to study the shoaling and breaking characteristics of irregular waves. Case 2 of this experiment was notable in that the peak frequency of the simulated wave spectrum was actually in fairly deep water ($kh=1.9$), well outside the probable range of validity for Boussinesq theory. The experimental setup is depicted in Figure 8, which was taken from Wei and Kirby.[20] Mase and Kirby[19] generated Pierson–Moskowitz spectra at the wavemaker in two different experiments; Case 2 had a peak frequency of 1 Hz. This choice of peak frequency, combined with the broad-banded spectral shape, allowed significant energy in frequencies that were well into the deep water range, thus providing a demanding test for dispersive shoaling models.

We will be taking the model through the surf zone, requiring implementation of a dissipation mechanism in our model. We use the methodology of Mase and Kirby[19] to formulate this dissipation, which revises (36) to:

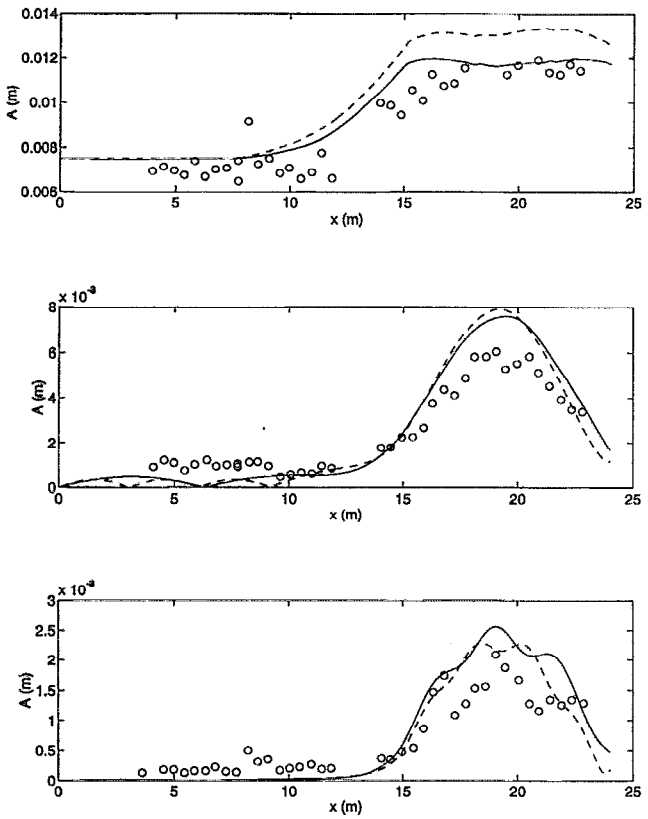

FIG. 5. Comparisons between models and Whalin's experiment, $T=2$ s, $a_0=0.75$ cm. Nonlinear mild-slope model (–), KP model of Liu *et al.*[4] (– –), data of Whalin[16] (O). (Top) first harmonic; (middle) second harmonic; (bottom) third harmonic.

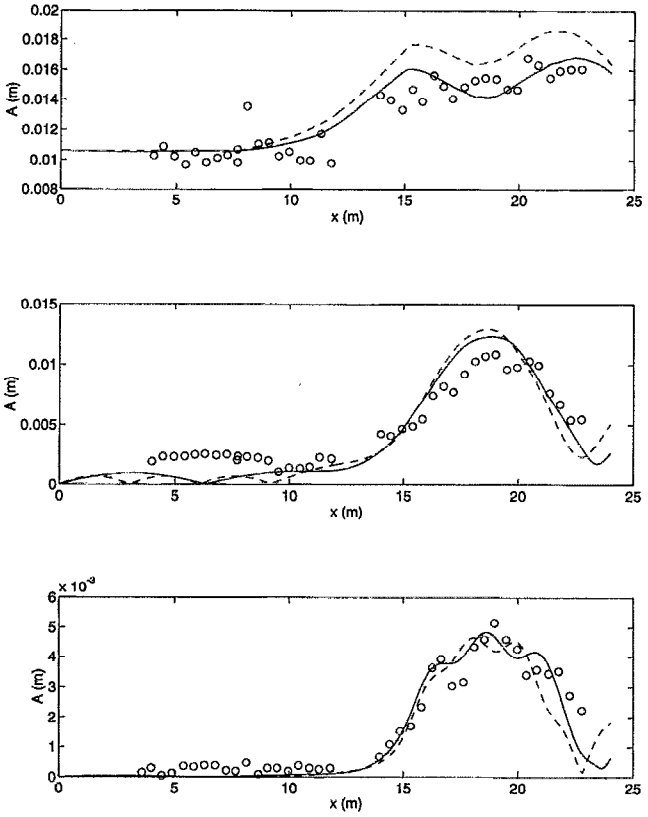

FIG. 6. Comparisons between models and Whalin's experiment, $T=2$ s, $a_0=1.06$ cm. Nonlinear mild-slope model (–), KP model of Liu *et al.*[4] (– –), data of Whalin[16] (O). (Top) first harmonic; (middle) second harmonic; (bottom) third harmonic.

$$A_{nx}+\frac{(kCC_g)_{nx}}{2(kCC_g)_n}A_n+\alpha_n A_n = -\frac{i}{8(kCC_g)_n}\left(\sum_{l=1}^{n-1} RA_l A_{n-l}e^{i\int(k_l+k_{n-l}-k_n)dx} + 2\sum_{l=1}^{N-n} SA_l^* A_{n+l}e^{i\int(k_{n+l}-k_l-k_n)dx}\right) \tag{37}$$

where:

$$\alpha_n=\alpha_{n0}+\left(\frac{f_n}{f_{\text{peak}}}\right)^2\alpha_{n1}, \tag{38}$$

$$\alpha_{n0}=F\beta(x), \tag{39}$$

$$\alpha_{n1}=(\beta(x)-\alpha_{n0})\frac{f_{\text{peak}}^2\Sigma_{n=1}^{N}|A_n|^2}{\Sigma_{n=1}^{N}f_n^2|A_n|^2}, \tag{40}$$

$$\beta(x)=\frac{3\sqrt{\pi}}{4\sqrt{gh}}\frac{B^3 f_{\text{peak}}H_{\text{rms}}^5}{\gamma^4 h^5}, \tag{41}$$

$$H_{\text{rms}}=2\sqrt{\sum_{n=1}^{N}|A_n|^2}, \tag{42}$$

and where f_{peak} is the peak frequency of the spectrum. The free parameters B, F and γ are assigned values of 1.0, 0.5 and 0.6, respectively. This was based on comparisons to the data of Mase and Kirby[19] and are close to values found from field data by Thornton and Guza.[21] The dissipation function (41) is the so-called "simple" probabilistic dissipation model of Thornton and Guza.[21] The frequency distribution of the dissipation mechanism is divided into α_{n0}, which drains an equal amount of energy across all frequencies, and α_{n1}, which weights the dissipation higher toward higher frequencies; this is shown in (38). The distribution α_{n1} represents the f^2 dissipation trend found from the data. A detailed derivation of this dissipation model is found in Mase and Kirby.[19] We will compare (37) to the "consistent" shoaling model of Freilich and Guza,[3] which was equipped with the same dissipation mechanism as described above.

Figures 9 through 12 show comparisons between the data, the nonlinear mild-slope model (37), and the "consistent" shoaling model. Most of the waves began to break at $h=17.5$ cm, so Figs. 11 and 12 detail the effectiveness of the dissipation function as well as that of the model equations. It is apparent that the nonlinear mild-slope model compares very well to the data for much of the frequency range throughout most of the domain. The "consistent" model, on the other hand, exhibits a strong deviation from the spectral peak even at the first slope gage ($d=35$ cm). This deviation is due to the overshoaling of frequency components in deeper water than that for which Green's Law (1) is valid. As the waves shoal and break, deviation of both models from the data becomes more pronounced. This may be due to pos-

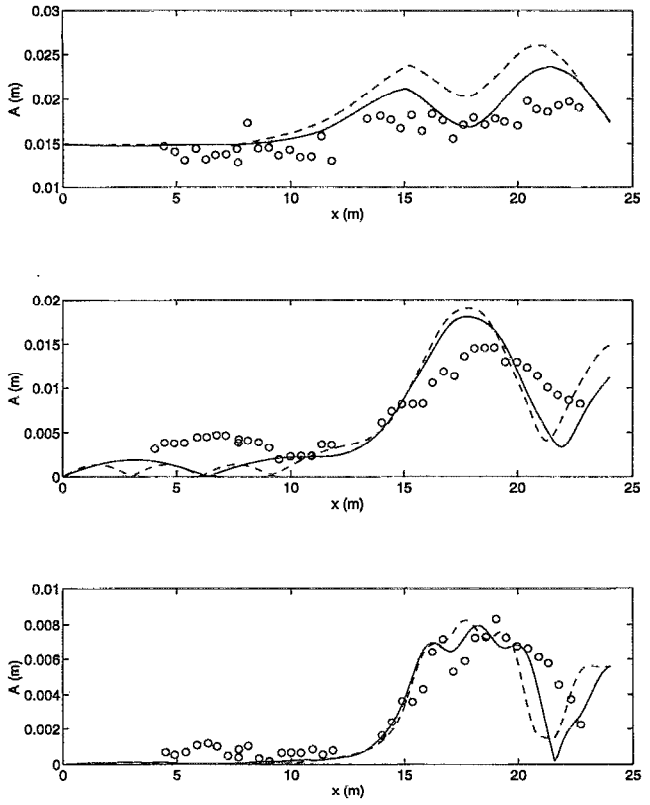

FIG. 7. Comparisons between models and Whalin's experiment, $T=2$ s, $a_0=1.49$ cm. Nonlinear mild-slope model (–), KP model of Liu *et al.*[4] (– –), data of Whalin[16] (O). (Top) first harmonic; (middle) second harmonic; (bottom) third harmonic.

sible inadequacies of the dissipation mechanism. Overall, however, one may conclude from both data-model comparisons that the parabolic nonlinear mild-slope model performs better than equivalent models with lowest-order dispersion and Green's Law shoaling. This is primarily due to the mild-slope formulation, which retains fully-dispersive linear theory for the dispersive and shoaling characteristics.

VI. SUMMARY

This study detailed the development of a nonlinear parabolic frequency-domain mild slope equation. The linear characteristics of the model utilize fully-dispersive linear theory,

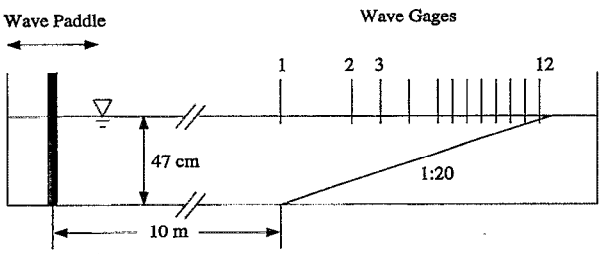

FIG. 8. Experimental setup of Mase and Kirby[19] (taken from Wei and Kirby[20]).

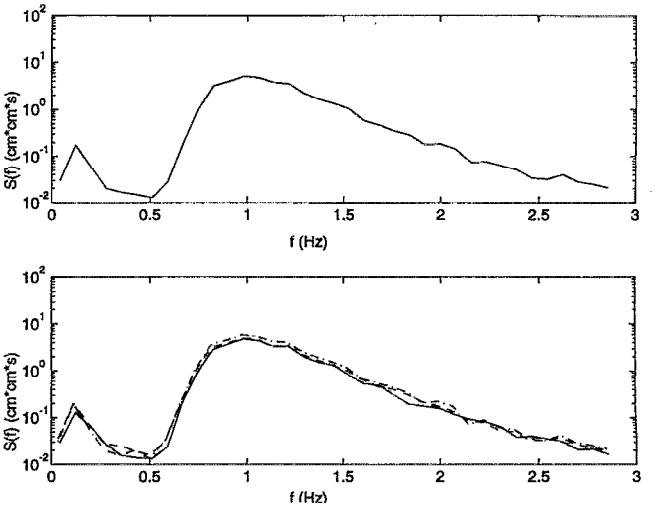

FIG. 9. Comparison of shoaling models to Case 2 of Mase and Kirby.[20] Experimental data (–), nonlinear mild-slope model (– –), consistent model of Freilich and Guza[3] (–·–). (Top) input spectra at $d=47$ cm; (bottom) $d=35$ cm.

thus insuring the validity of the linear terms of the model in arbitrary water depth. This represents an advance over frequency-domain Boussinesq models, which are weakly dispersive and thus limited to shallow water. The resulting

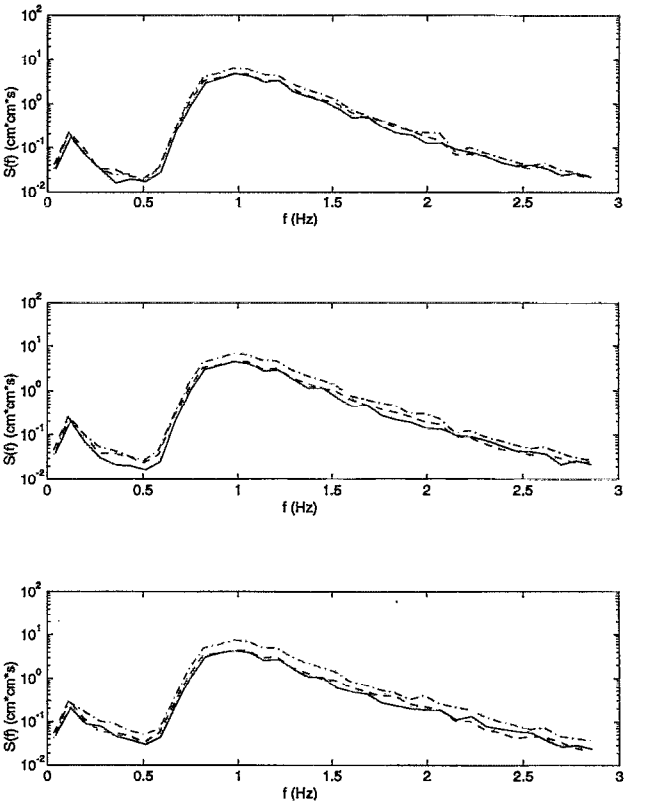

FIG. 10. Comparison of shoaling models to Case 2 of Mase and Kirby.[19] Experimental data (–), nonlinear mild-slope model (– –), consistent model of Freilich and Guza[3] (–·–). (Top) $d=30$ cm; (middle) $d=25$ cm; (bottom) $d=20$ cm.

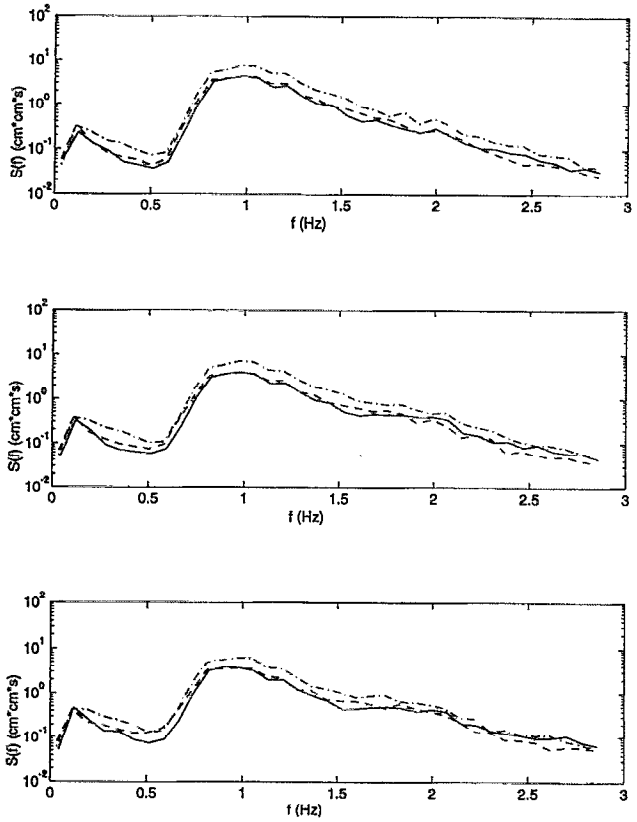

FIG. 11. Comparison of shoaling models to Case 2 of Mase and Kirby.[19] Experimental data (–), nonlinear mild-slope model (– –), consistent model of Freilich and Guza[3] (–·–). (Top) $d=17.5$ cm; (middle) $d=15$ cm; (bottom) $d=12.5$ cm.

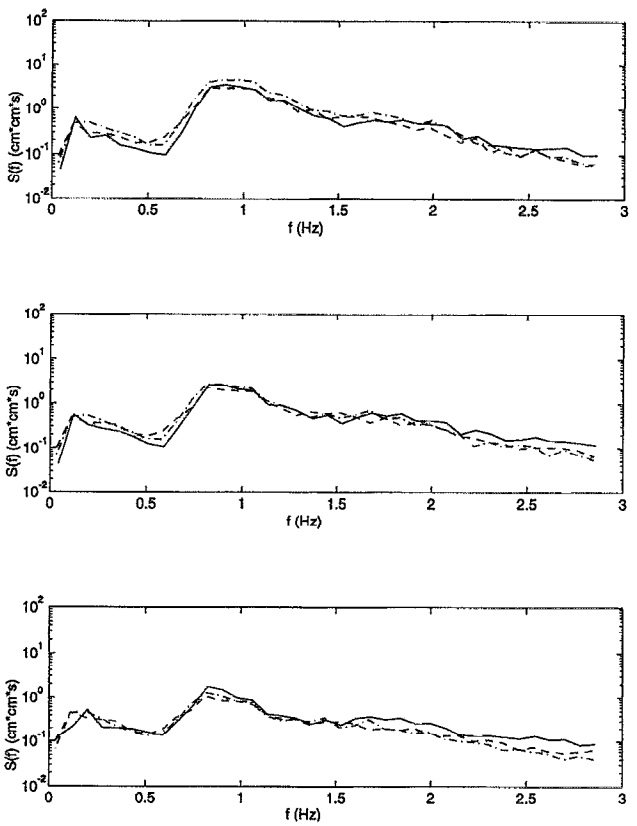

FIG. 12. Comparison of shoaling models to Case 2 of Mase and Kirby.[19] Experimental data (–), nonlinear mild-slope model (– –), consistent model of Freilich and Guza[3] (–·–). (Top) $d=10.0$ cm; (middle) $d=7.5$ cm; (bottom) $d=5$ cm.

model was compared to experimental data and a frequency-domain Boussinesq model. In general the present model demonstrated improved comparisons with the data over the Boussinesq model, especially in instances where the data were outside the shallow water range. This was especially apparent in the comparisons to the data of Mase and Kirby,[19] where most of the frequencies were in intermediate or deep water. We also added a surf zone dissipation mechanism to the model to enhance the comparisons to the experiment of Mase and Kirby.[19]

One drawback of the parabolic formulation used in this study is the limitation to small angles of incidence. Future work will likely involve overcoming this limitation and investigating other possible dissipation mechanisms, as well as generalizing this dissipation to two horizontal dimensions.

ACKNOWLEDGMENTS

The first author was supported by an ASEE National Science and Engineering Graduate Fellowship from the Office of Naval Research while a Ph.D. candidate at the University of Delaware. The second author was supported by University Research Initiative Grant No. DAAL-03-92-G0116 from the Army Research Office.

APPENDIX: LAGRANGIAN DERIVATION OF THE MODEL IN A NONSTATIONARY DOMAIN

1. Lagrangian derivation of Equation (20)

A variational principle governing the motion of fluid described by (2) is given by Luke:[22]

$$\delta\int_t\int_{\mathbf{x}} L(\eta,\phi;\mathbf{x},t)d\mathbf{x}dt=0, \tag{A1}$$

where

$$L=\int_{-h}^{\eta}\rho\left\{gz+\phi_t+\frac{1}{2}(\nabla_h\phi)^2+\frac{1}{2}(\phi_z)^2\right\}dz \tag{A2}$$

is the Lagrangian density of the motion, and $\{\mathbf{x},t\}$ is the propagation space of the waves. Since variations of L with respect to arbitrary $\delta\phi$ and $\delta\eta$ will reduce L by one order of ϵ, we need to retain terms to $O(\epsilon^3)$ in L, after which linear terms will arise due to variations of $O(\epsilon^2)$ quantities of L.. Taking η and ϕ to be $O(\epsilon)$ and expanding L about $z=0$ then gives

$$\frac{L}{\rho}=\frac{g\eta^2}{2}+\frac{1}{2}\int_{-h}^{0}(\nabla_h\phi)^2dz+\frac{1}{2}\int_{-h}^{0}(\phi_z)^2dz + \eta\left\{\phi_t+\frac{\eta}{2}\phi_{zt}+\frac{1}{2}(\nabla_h\phi)^2+\frac{1}{2}(\phi_z)^2\right\}\Big|_{z=0}. \tag{A3}$$

Variation of L with respect to η gives the dynamic free surface boundary condition (8) directly. Varying L with respect to ϕ then yields

$$\int_t\int_{\mathbf{x}}\Big\{\int_{-h}^{0}\nabla_h\phi\cdot\nabla_h(\delta\phi)dz+\int_{-h}^{0}\phi_z(\delta\phi)_z dz+\eta(\delta\phi)_t\Big|_{z=0}+\eta\nabla_h\phi\cdot\nabla_h(\delta\phi)\Big|_{z=0}\Big\}d\mathbf{x}dt+\int_t\int_{\mathbf{x}}\Big\{\frac{\eta^2}{2}(\delta\phi)_{zt}+\eta\phi_z(\delta\phi)_z\Big\}\Big|_{z=0}d\mathbf{x}dt. \tag{A4}$$

After one partial integration, the integrand of the second integral becomes

$$\eta\{-\eta_t+\phi_z\}\Big|_{z=0}(\delta\phi)_z=O(\epsilon^4) \tag{A5}$$

due to (5). The remainder of the equation can be manipulated by recognizing that only terms proportional to ϕ_n^2 in the $O(\epsilon^2)$ portion of (A4) will contribute to the linear portion of equations for ϕ_n after variations with respect to ϕ_n. We can then write (A4) as:

$$\int_t\int_{\mathbf{x}}\Big[\Big\{-\nabla_h\cdot\int_{-h}^{0}f_n^2dz\nabla_h\tilde{\phi}_n+\int_{-h}^{0}f_n^2dz\tilde{\phi}_n-\eta_{n_t}\Big\}(\delta\tilde{\phi}_n)-\nabla_h\cdot(\eta\nabla_h\phi)(\delta\phi)\Big|_{z=0}\Big]d\mathbf{x}dt=0, \tag{A6}$$

where we must set $\delta\phi|_{z=0}=\delta\tilde{\phi}_n$ to obtain nonlinear terms contributing to the $\tilde{\phi}_n$ components. Substituting for η_{n_t} from (8) then gives

$$\tilde{\phi}_{n_{tt}}-\nabla_h\cdot[(CC_g)_n\nabla_h\tilde{\phi}_n]+\omega_n^2\Big(1-\frac{C_{gn}}{C_n}\Big)\tilde{\phi}_n=\Big\{-\nabla_h\cdot(\phi_t\nabla_h\phi)-\frac{1}{2}(\nabla_h\phi)_t^2-\frac{1}{2}(\phi_z)_t^2+\frac{1}{2g}(\phi_t)_{zt}^2\Big\}_n\Big|_{z=0}, \tag{A7}$$

where we have used (16) through (19). Substituting for ϕ from (10) then gives (20).

2. A nonstationary domain: Effect of ambient currents

The results of the preceding section may be conveniently extended to the case of a moving domain containing an ambient current $\mathbf{U}(x,y)=\{U,V\}=\nabla_h\phi_0$. The current is assumed to be constant over depth, consistent with irrotationality and a slowly varying depth $h(x,y)$. It is further assumed that $\mathbf{U}=\nabla_h\phi_0=O(1)$; the solution to $O(\epsilon)$ for a single wave component from (10) is then known to be

$$\phi=\phi_0+f_n(k_n,h,z)\tilde{\phi}_n(k_n,\omega_n,x,y,t) \tag{A8}$$

with

$$\tilde{\phi}_n=\frac{-igA_n}{2\sigma_n}e^{i\{\int\mathbf{k}_n\cdot dx-\omega_n t\}}+c.c. \tag{A9}$$

for progressive waves. The absolute frequency ω_n may be written in terms of the intrinsic frequency σ_n according to

$$\omega_n=\sigma_n+\mathbf{k}_n\cdot\mathbf{U}, \tag{A10}$$

where

$$\sigma_n=(gk_n\tanh k_nh)^{1/2}. \tag{A11}$$

We proceed to $O(\epsilon^2)$ by assuming forms for ϕ and η according to

$$\phi=\phi_0+(\epsilon)\sum_n f_n(k_n,h,z)\tilde{\phi}_n(k_n,\omega_n,x,y,t)+O(\epsilon,\tilde{\alpha})=\phi_0+(\epsilon)\phi_1, \tag{A12}$$

$$\eta=\eta_0+(\epsilon)\eta_1. \tag{A13}$$

Here, η_0 represents the $O(1)$ setdown due to the strong current $\mathbf{U}$. The $O(1)$ water depth is thus given by $h=h_0+\eta_0$, where now h_0 is the still water depth. We use the Lagrangian approach of this appendix. Accordingly, (A12) and (A13) are substituted into (A1) to obtain

$$L/\rho=L_0'+(\epsilon)L_1'+(\epsilon^2)L_2' \tag{A14}$$

where

$$L_0'=g\frac{(\eta_0^2-h_0^2)}{2}+\tfrac{1}{2}|\mathbf{U}|^2(\eta_0+h_0), \tag{A15}$$

$$L_1'=g\eta_0\eta_1+\int_{h_0}^{\eta_0}(\phi_{1_t}+\mathbf{U}\cdot\nabla_h\phi_1)dz+\frac{1}{2}|\mathbf{U}|^2\eta_1, \tag{A16}$$

$$L_2'=\frac{g\eta_1^2}{2}+\frac{1}{2}\int_{-h_0}^{\eta_0}((\nabla_h\phi_1)^2+(\phi_{1_z})^2)dz+(\phi_{1_t}+\mathbf{U}\cdot\nabla_h\phi_1)\Big|_{\eta_0}^{\eta_1}+(\epsilon)\Big[\{\phi_{1_t}+\mathbf{U}\cdot\nabla_h\phi_1\}_z\Big|_{\eta_0}\frac{\eta_1^2}{2}+\frac{1}{2}[(\nabla_h\phi_1)^2+(\phi_{1_z})^2]_{\eta_0}\eta_1\Big]. \tag{A17}$$

Variations of the integral of L_0' with respect to η_0 and ϕ_0 yield the relations

$$\eta_0=-\frac{1}{2g}|\mathbf{U}|^2, \tag{A18}$$

$$\nabla_h\cdot\{(h_0+\eta_0)\mathbf{U}\}=0, \tag{A19}$$

as required for a steady current. L_2' is altered from (A3) by the advective term. Variation with respect to η_1 yields the dynamic boundary condition

$$g\eta_1+\Big\{\frac{D\phi_1}{Dt}+\eta_1\Big(\frac{D\phi_1}{Dt}\Big)_z+\frac{1}{2}(\nabla_h\phi_1)^2+\tfrac{1}{2}(\phi_{1z})^2\Big\}\Big|_{\eta_0}=O(\epsilon^3). \tag{A20}$$

Varying the integral (A17) by ϕ_1 and eliminating the kinematic boundary condition yields

$$\int_t\int_x\Bigg[\int_{-h_0}^{\eta_0}\nabla_h\phi_1\cdot\nabla_h(\delta\phi_1)dz+\int_{-h_0}^{\eta_0}\phi_{1_z}(\delta\phi_1)_z dz - \left\{\frac{D\eta_1}{Dt}+(\nabla_h\cdot\mathbf{U})\eta_1\right\}(\delta\phi_1)\Bigg|_{\eta_0}-\nabla_h\cdot(\eta_1\nabla_h\phi_1)\Bigg|_{\eta_0} -\frac{\eta_1^2}{2}(\nabla_h\cdot\mathbf{U})(\delta\phi_1)_z\Bigg|_{\eta_0}\Bigg]d\mathbf{x}dt=0, \tag{A21}$$

where the last term is $O(\epsilon^3,\alpha)\sim O(\epsilon^4)$ due to (A19). The operator

$$\frac{D}{Dt}\equiv\frac{\partial}{\partial t}+\mathbf{U}\cdot\nabla_h\cdot$$

Eliminating η_1 and substituting the expansion of ϕ_1 from (A12) gives the desired form of the wave equation for the n'th component at ω_n:

$$\frac{D^2\tilde{\phi}_n}{Dt^2}+(\nabla_h\cdot\mathbf{U})\frac{D\tilde{\phi}_n}{Dt}-\nabla_h\cdot\{(CC_g)_n\nabla_h\tilde{\phi}_n\} +(\sigma^2-k^2CC_g)_n\tilde{\phi}_n =\frac{1}{2}\Bigg[\sum_l\sum_m\left\{\frac{\sigma_l^2+\sigma_m^2}{g^2}\frac{D}{Dt}\left(\frac{D\tilde{\phi}_l}{Dt}\frac{D\tilde{\phi}_m}{Dt}\right) -\frac{\sigma_m^2}{g^2}\frac{D}{Dt}(\tilde{\phi}_l\tilde{\phi}_n)\sigma_l^2\right\}-\sum_l\sum_m\left\{\frac{D}{Dt}(\nabla_h\tilde{\phi}_l\cdot\nabla_h\tilde{\phi}_m) +\nabla_h\cdot\left(\frac{D\tilde{\phi}_l}{Dt}\nabla_h\tilde{\phi}_m\right)+\nabla_h\cdot\left(\frac{D\tilde{\phi}_m}{Dt}\nabla_h\tilde{\phi}_l\right)\right\}\Bigg]_n. \tag{A22}$$

This extends (20) to include an ambient current $\mathbf{U}$ where $k\mathbf{U}/\omega=O(1)$. The linearized form of (A22) is the wave–current equation of Kirby.[23] Proceeding directly to the coupled parabolic equations following the method of section II, we obtain

$$2i\sigma_n(C_{gn}+U)A_{n_x}-2\sigma_n(C_{gn}+U)(\tilde{k}_n-k_n)A_n +i\sigma_n^2\left\{\left(\frac{C_{gn}+U}{\sigma_n}\right)_x+\left(\frac{V}{\sigma_n}\right)_y\right\}A_n+\sigma_n\left\{(CC_g)_n\left(\frac{A_n}{\sigma_n}\right)_y\right\}_y =\frac{1}{4}\sum_l R'A_lA_{n-l}e^{i(k_{l_0}+k_{n-l_0}-k_{n_0})x} +\frac{1}{2}\sum_l S'A_lA_{n+l}e^{i(k_{n+l_0}-k_{l_0}-k_{n_0})x}, \tag{A23}$$

where $R'=R(\sigma_n,\sigma_{n-l},\sigma_l,k_{n-l},k_l)$ and so on. The linearized, one-dimensional (in x) form of (A23) is equivalent to the linearized form of the wave-current equation of Turpin *et al.*[24] after neglecting time dependence. In this derivation, we have assumed that waves propagate primarily in the x-direction, and we have further restricted the large current assumption by specifying that

$$\frac{|U|^2}{CC_g}\sim O(\epsilon) \tag{A24}$$

as in Kirby[23] and Booij.[25] Consistent with the first assumption, it would be appropriate to calculate σ_n according to

$$\sigma_n=\omega_n-k_nU \tag{A25}$$

since propagation has been assumed to be nearly colinear with the x-direction.

[1] D.H. Peregrine, "Long waves on a beach," J. Fluid Mech. **27**, 815 (1967).
[2] O.B. Rygg, "Nonlinear refraction-diffraction of surface waves in intermediate and shallow water," Coast. Eng. **12**, 191 (1988).
[3] M.H. Freilich and R.T. Guza, "Nonlinear effects on shoaling surface gravity waves," Proc. R. Soc. London Ser. A **311**, 1 (1984).
[4] P. L.-F. Liu, S.B. Yoon, and J.T. Kirby, "Nonlinear refraction-diffraction of waves in shallow water," J. Fluid Mech. **153**, 185 (1985).
[5] J.T. Kirby, "Modelling shoaling directional wave spectra in shallow water," *Proceedings of the 22nd International Conference on Coastal Engineering*, Delft, the Netherlands, 1990 (American Society of Civil Engineers, New York, 1990), pp. 109–121.
[6] P.J. Bryant, "Periodic waves in shallow water," J. Fluid Mech. **59**, 625 (1973).
[7] P.J. Bryant, "Stability of periodic waves in shallow water," J. Fluid Mech. **66**, 81 (1974).
[8] J.B. Keller, "Resonantly interacting water waves," J. Fluid Mech. **191**, 529 (1988).
[9] Y. Agnon, A. Sheremet, J. Gonsalves, and M. Stiassnie, "Nonlinear evolution of a unidirectional shoaling wave field," Coast. Eng. **20**, 29 (1993).
[10] R. Smith and T. Sprinks, "Scattering of surface waves by a conical island," J. Fluid Mech. **72**, 373 (1975).
[11] O.M. Phillips, *The Dynamics of the Upper Ocean*, 2nd edition (Cambridge University Press, Cambridge, 1980).
[12] J.C.W. Berkhoff, "Computation of combined refraction-diffraction," *Proceedings of the 13th International Conference on Coastal Engineering*, Vancouver, British Columbia, Canada (American Society of Civil Engineers, New York, 1972), pp. 471–490.
[13] A.C. Radder, "On the parabolic equation method for water-wave propagation," J. Fluid Mech. **95**, 159 (1979).
[14] C. J. Lozano and P. L.-F. Liu, "Refraction–diffraction model for linear surface water waves," J. Fluid Mech. **101**, 705 (1980).
[15] D.K.P. Yue and C.C. Mei, "Forward diffraction of Stokes waves by a thin wedge," J. Fluid Mech. **99**, 33 (1980).
[16] R.W. Whalin, "The limit of application of linear wave refraction theory in a convergence zone," Research Report No. H-71-3, U.S. Army Engineer Waterways Experiment Station, Vicksburg, MS, 1971.
[17] P.A. Madsen and O. R. Sørensen, "A new form of the Boussinesq equations with improved linear dispersion characteristics. Part 2. A slowly-varying bathymetry," Coast. Eng. **18**, 183 (1992).
[18] O. Nwogu, "Nonlinear transformation of multi-directional waves in water of variable depth," unpublished manuscript (1994).
[19] H. Mase and J.T. Kirby, "Hybrid frequency-domain KdV equation for random wave transformation," *Proceedings of the 23rd International Conference on Coastal Engineering*, Venice, Italy (American Society of Civil Engineers, New York, 1992), pp. 474–487.
[20] G. Wei and J.T. Kirby, "A time-dependent numerical code for extended Boussinesq equations," J. Waterways, Port, Coast. Ocean. Eng. (ASCE), in press (1994).
[21] E.B. Thornton and R.T. Guza, "Transformation of wave height distribution," J. Geophys. Res. **88**, 5925 (1983).

[22]J.C. Luke, "A variational principle for a fluid with a free surface," J. Fluid Mech. **27**, 395 (1967).
[23]J.T. Kirby, "A note on linear surface wave–current interaction over slowly varying bathymetry," J. Geophys. Res. **89**, 745 (1984).
[24]F.-M. Turpin, C. Benmoussa, and C.C. Mei, "Effects of slowly varying depth and current on the evolution of a Stokes wavepacket," J. Fluid Mech. **132**, 1 (1983).
[25]N. Booij, "Gravity waves on water with non-uniform depth and current," Report No. 81-1, Department of Civil Engineering, Delft University of Technology, Delft, the Netherlands, 1981.